Engineered disulfide crosslinking to measure conformational changes in the 26S proteasome

Randi G. Reed, Robert J. Tomko Jr.[*]

Department of Biomedical Sciences, Florida State University College of Medicine, Tallahassee, FL, United States
*Corresponding author: e-mail address: robert.tomko@med.fsu.edu

Contents

Abstract

The 26S proteasome is a multisubunit ATP-dependent peptidase complex mediating most regulated protein degradation in eukaryotes. The proteasome undergoes several coordinated conformational changes during catalysis that activate it for substrate processing and functionally couple distinct enzymatic activities during substrate degradation. Understanding the impact of substrate interactions and individual ATP binding events on these conformational changes is currently a major bottleneck in the study of proteasome function. Here, we describe a simple biochemical reporter based on engineered disulfide crosslinking for measuring the conformational distribution of the *Saccharomyces cerevisiae* 26S proteasome. We demonstrate its use to investigate the impact of ATP analogs and proteasome inhibitors on proteasome conformational equilibria. This reporter allows simultaneous and rapid comparison of multiple treatments or conditions on the steady-state conformational distribution of the proteasome and can be readily extended to the study of other multisubunit complexes for which multiple conformational states are known at near-atomic resolution.
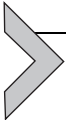
1. Introduction

The 26S proteasome is a 2.5-MDa ATP-dependent peptidase complex responsible for most regulated intracellular degradation in eukaryotes (Bard, Goodall, et al., 2018; Finley, Chen, & Walters, 2016; Tomko & Hochstrasser, 2013). It consists of a barrel-shaped, proteolytic core particle (CP) capped on one or both ends by a 19S regulatory particle (RP) (Fig. 1A). The RP can be further subdivided into two subcomplexes, the lid and the base. The lid consists of Rpn3, 5–9, 11, 12, and Rpn15/Sem1 subunits. The base consists of non–ATPase subunits Rpn1, 2, and 13, and a hexameric ring of six ATPase subunits, Rpt1–Rpt6. Rpn1, Rpn13, and an additional subunit, Rpn10, serve as receptors for incoming substrates. During substrate processing, the Rpn11 lid subunit removes the polyubiquitin targeting
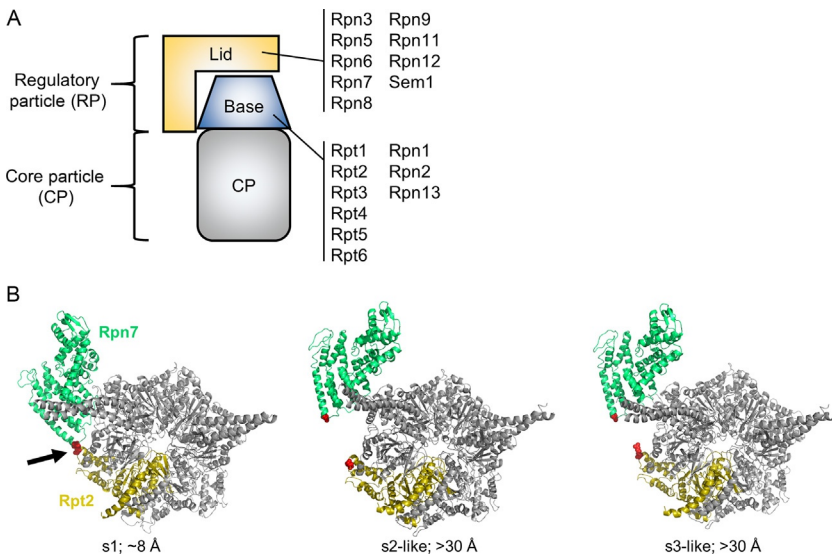

Fig. 1 (A) Cartoon depiction of the 26S proteasome. The subunit composition of the lid and base subcomplexes is shown. (B) Rpn7-D123 and Rpt2-R407 are juxtaposed in the s1 conformation of the yeast 26S proteasome (*red spheres* indicated by *arrow*) (PDB 4CR2), but are distant in the s2–s6 states. In the *middle panel*, the s2 state (PDB 4CR3) is shown, but the s5 state is highly similar. In the *right panel*, the s3 state (PDB 4CR4) is shown, but the s4 and s6 states are highly similar. The approximate distances in angstroms between the Rpn7-D123 and Rpt2-R407 alpha carbons are shown. *Panel (B) is modified from Eisele, M. R., Reed, R. G., Rudack, T., Schweitzer, A., Beck, F., Nagy, I., et al. (2018). Expanded coverage of the 26S proteasome conformational landscape reveals mechanisms of peptidase gating.* Cell Reports, 24(5), 1301–1315.e5. doi:10.1016/j.celrep.2018.07.004 *with permission from Elsevier.*

signal (Verma et al., 2002; Worden, Dong, & Martin, 2017; Yao & Cohen, 2002). The base unfolds the substrate and translocates it through the central pore of the ATPase ring to the peptidase active sites of the CP, where it is cleaved into short peptides.

An onslaught of recent cryo–electron microscopy (cryo–EM) analyses has demonstrated that 26S proteasomes can adopt at least six conformational states, herein referred to as s1–s6 (Asano et al., 2015; Aufderheide et al., 2015; Bashore et al., 2015; Chen et al., 2016; de la Pena, Goodall, Gates, Lander, & Martin, 2018; Dong et al., 2018; Eisele et al., 2018; Guo et al., 2018; Haselbach et al., 2017; Huang, Luan, Wu, & Shi, 2016; Luan et al., 2016; Matyskiela, Lander, & Martin, 2013; Schweitzer et al., 2016; Sledz et al., 2013; Unverdorben et al., 2014; Wehmer et al., 2017; Zhu et al., 2018) (reviewed in Bard, Goodall, et al., 2018). These states can be broadly grouped into three categories: s1, s2-like, and s3-like. The s1 state appears to be the ground or resting state of the proteasome, and it is believed to be the major substrate-accepting state. In the s2-like states, the lid subcomplex undergoes a rotation that positions the deubiquitinase subunit Rpn11 directly over the pore of the ATPase ring of the base for substrate deubiquitination (Matyskiela et al., 2013; Sledz et al., 2013). Although these states appear primed for deubiquitination, a mismatch between the pore of the ATPase ring and the central channel of the CP suggests that they may not be fully competent for substrate degradation (Eisele et al., 2018; Unverdorben et al., 2014). Finally, in the s3-like states, the ATPase ring undergoes move-ments that align its pore with the central channel of the CP, providing an unobstructed passageway for processing and delivery of the substrate into the peptidase sites (Chen et al., 2016; de la Pena et al., 2018; Dong et al., 2018; Eisele et al., 2018; Luan et al., 2016; Matyskiela et al., 2013; Sledz et al., 2013; Unverdorben et al., 2014; Wehmer et al., 2017). Thus, the s3-like states represent actively processing proteasomes (de la Pena et al., 2018; Eisele et al., 2018; Matyskiela et al., 2013). Although these cryo–EM structures have been groundbreaking in terms of visualizing the substrate processing mechanism of the proteasome, the events and signals that promote each of these rearrangements remain poorly understood (Bard, Bashore, Dong, & Martin, 2018; Bard, Goodall, et al., 2018; Eisele et al., 2018).

The large-scale repositioning of the lid relative to the base that occurs as the proteasome shifts from the resting s1 state to the s2/s3-like states results in the formation and breakage of specific molecular contacts between lid and base subunits (for example, see Fig. 1B). Such dynamic contacts can serve as reporters to discriminate the resting s1 state from the s2/s3-like states, permitting measurement of the fraction of resting vs activated

proteasomes. Engineered disulfide crosslinking has previously been used to assay static interactions between adjacent subunits within the proteasome (Tomko, Funakoshi, Schneider, Wang, & Hochstrasser, 2010; Velichutina, Connerly, Arendt, Li, & Hochstrasser, 2004). Here, we apply this approach to dynamic subunit–subunit contacts to measure the relative fraction of s1 proteasomes. We demonstrate the use of this method for assessing the impact of ATP analogs and proteasome inhibitors on the conformational distribution of 26S proteasomes in yeast whole cell extracts (WCE). This approach is simple, rapid, and can be readily implemented for studying the conformational dynamics of other large protein complexes that adopt multiple conformational states.
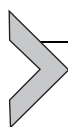
2. Assessing the impact of ATP analogs on 26S proteasome conformational distribution

We have found that conformation–specific crosslinking performed in WCE accurately reports on the conformation of 26S proteasomes with little to no influence from proteasome assembly intermediates. This is because the abundances of assembly intermediates are typically very low compared to the abundance of 26S proteasomes. For initial analyses, we prefer yeast strains harboring cysteine substitutions at Rpn7-D123 and Rpt2-R407 for crosslinking because these mutations have no obvious impact on proteasome structure, assembly, or function, and the spacing of these residues increases substantially between the s1 and s2-/s3-like states (Fig. 1B). However, other substitutions can also be used if the cysteine substitutions are well tolerated and are appropriately juxtaposed in the s1 state but not the s2- or s3-like states. We have also successfully utilized Rpn6 (T203C)–Rpt6(G387C) and Rpn7(A236C)–Rpt6(R339C) substitution pairs (Eisele et al., 2018; unpublished observations). These pairs do not obviously compromise proteasome structure or function and respond to ATP analogs similarly to the Rpn7(D123C)–Rpt2(R407C) pair. Site-directed mutagenesis to introduce cysteine substitutions is not covered here.

2.1 Materials
Unless listed below, all reagents are purchased from Millipore Sigma.
- Zymolyase buffer (ZB): $1.2\,M$ D-sorbitol, $50\,mM$ Tris–HCl, pH 8.0, and $500\,\mu M$ MgCl$_2$ dissolved in deionized water. This reagent can be stored at room temperature indefinitely (Table 1).
- $1\,M$ dithiothreitol (DTT): dissolve in deionized water. This reagent can be stored in small aliquots for at least a year at $-20°C$.

Table 1 Concentrations of key reagents used during extract preparation and crosslinking

Reagent	Stock concentration	Final concentration
For spheroplasting		
DTT	$1 M$	$30 \text{ m}M$
Zymolyase 20T	20 mg/mL	0.8 mg/mL
For cell lysis		
ATP	$100 \text{ m}M$	$2 \text{ m}M$
ATPγS	$100 \text{ m}M$	$2 \text{ m}M$
AMP-PNP	$100 \text{ m}M$	$2 \text{ m}M$
For crosslinking		
CuCl$_2$	$10 \text{ m}M$	$250 \text{ μ}M$
NEM	$200 \text{ m}M$	$10 \text{ m}M$
EDTA	$100 \text{ m}M$	$10 \text{ m}M$
DTT (reduced control only)	$1 M$	$20 \text{ m}M$

- 20 mg/mL Zymolyase 20T (MP Biomedicals): dissolve Zymolyase 20T in ZB. This reagent can be stored in small aliquots at −20°C for at least a year, and working stocks can be kept refrigerated for at least 3 months.
- Lysis buffer (LB): 50 mM HEPES–NaOH, pH 7.5, 150 mM NaCl, and 5 mM MgCl$_2$. This reagent can be stored at room temperature indefinitely. Nucleotides are added from a concentrated stock immediately before use.
- Protein concentration assay reagent (such as Bio-Rad Protein Assay Reagent or similar).
- 100 mM adenosine triphosphate disodium salt hydrate (ATP): dissolve in 50 mM Tris–HCl, pH 7.5. Store as single-use aliquots at −80°C. This reagent is stable for at least 6 months.
- 100 mM adenosine 5′-(3-thiotriphosphate) tetralithium salt (ATPγS): dissolve in 50 mM Tris–Cl, pH 7.5. Store as single-use aliquots at −80°C. This reagent is stable for at least 6 months.
- 100 mM adenosine 5′-(β,γ-imido)triphosphate lithium salt hydrate (AMP-PNP): dissolve in 50 mM Tris–Cl, pH 7.5. Store as single-use aliquots at −80°C. This reagent is stable for at least 6 months.
- 10 mM CuCl$_2$ prepared in deionized water. This reagent can be stored at room temperature indefinitely.

- 200 mM N-ethylmaleimide (NEM) prepared in 95% ethanol. This reagent can be stored at $-20°C$ for up to 1 week.
- 100 mM EDTA disodium salt dihydrate prepared in deionized water, pH 8.0. This reagent can be stored at room temperature indefinitely.
- $5 \times$ nonreducing loading buffer: 300 mM Tris–Cl, pH 6.8, 10% SDS, 50% glycerol, and 0.04% bromophenol blue. This reagent can be stored at $-20°C$ indefinitely.
- Congenic yeast strains harboring appropriate single or double cysteine substitutions, such as RTY2091 (*RPN7-D123C-6xGly-V5:kanMX6*), RTY2099 (*RPT2-R407C:natMX4*), and RTY2112 (*RPN7-D123C-6xGly-V5:kanMX6 RPT2-R407C:natMX4*) (Eisele et al., 2018).
- Antibodies against V5 tag (Life Technologies) and glucose-6–phosphate dehydrogenase (G6PD) (Millipore Sigma).

2.2 Equipment

- Absorbance spectrophotometer and appropriate cuvettes
- SDS–PAGE electrophoresis equipment (such as Bio-Rad Mini-PROTEAN3 system or similar)
- Electrotransfer apparatus (such as Bio-Rad Mini Trans-Blot or similar)
- Chemiluminescence imaging station (such as Bio-Rad Chemidoc MP or similar)
- Refrigerated microcentrifuge accepting 1.5 mL Eppendorf tubes
- Heat blocks or water baths set at 25°C and 100°C

2.3 Procedure

2.3.1 Cell growth, spheroplasting, and lysis

1. Inoculate 3 mL of YPD medium with each reporter strain from a colony on a freshly streaked YPD plate and incubate overnight at 30°C with aeration.
2. The following morning, use the overnight culture to inoculate 15 mL of YPD at an optical density of $OD_{600} \approx 0.2$. Incubate at 30°C with aeration.
3. Monitor cell growth via OD_{600}. At $OD_{600} \approx 1.0$, harvest 10 mL of cell culture in a 15-mL disposable conical tube. Centrifuge cells at $4000 \times g$ for 2 min at room temperature.
4. Aspirate the supernatant and resuspend the cell pellet in 1 mL of deionized water. Transfer the cell suspension to a 1.5-mL centrifuge tube. Centrifuge the cells at $10,000 \times g$ for 30 s to pellet cells.

5. Repeat the wash in step 4.
6. Aspirate the supernatant and resuspend the cells in $100\,\mu L$ ZB supplemented with $3\,\mu L$ of $1\,M$ DTT. Incubate at room temperature for 15 min.
7. Pellet cells at $10,000 \times g$ for 30 s at room temperature and discard the supernatant.
8. Resuspend the pellet in $100\,\mu L$ ZB and add $4\,\mu L$ of 20 mg/mL Zymolyase 20T. Mix, and incubate at 30°C for 30 min with gentle agitation to keep cells in suspension.
9. Gently pellet the spheroplasts by centrifuging at $1200 \times g$ for 1 min at room temperature (see Note 1). Resuspend the pellet in $200\,\mu L$ ZB. Break up the pellet by gently stirring with a wide-bore pipette tip and slowly pipetting up and down. Pellet the cells at $1200 \times g$ for 1 min at room temperature. Discard the supernatant.
10. Add $150\,\mu L$ of ice-cold LB containing $2\,mM$ of the desired nucleotide (see Note 2). Stir the pellet with a pipette tip to partially resuspend the cells.
11. Lyse the spheroplasts by vortexing three times for 30 s at top speed, leaving on ice for 1 min in between vortexings.
12. Pellet cell debris and unbroken cells at $21,000 \times g$ for 10 min at 4°C and transfer the supernatant to a fresh 1.5-mL centrifuge tube.
13. Perform a protein concentration assay on a small aliquot of the cleared WCE following manufacturer's instructions to determine the protein concentration. Adjust all sample concentrations to the least concentrated sample using LB containing the appropriate nucleotide (see Note 3).

2.3.2 Crosslinking of WCE

1. Transfer $50\,\mu L$ of the normalized WCE from Section 2.3.1, step 13 to a fresh Eppendorf tube containing $2.5\,\mu L$ of $200\,mM$ NEM. Add $5.25\,\mu L$ of $100\,mM$ EDTA, mix well, and store sample at $-80°C$ until analysis. This sample will serve as the noncrosslinked control.
2. Transfer $50\,\mu L$ of the remaining WCE from Section 2.3.1, step 13 to a fresh tube. Add $1.25\,\mu L$ of $10\,mM$ $CuCl_2$ to the lysate and mix gently but thoroughly to initiate crosslinking (see Note 4). Immediately place tubes in a 25°C water bath to maintain temperature (see Note 5).
3. After 10 min, add $2.5\,\mu L$ of $200\,mM$ NEM and $5.25\,\mu L$ of $100\,mM$ EDTA to terminate further crosslinking (see Note 6). Mix well.

4. For a control to demonstrate the reversibility of disulfide formation, add 1 μL of 1 M DTT to 50 μL of crosslinked WCE. Incubate sample for 10 min at room temperature before adding 2.5 μL of 200 mM NEM and 5.25 μL of 100 mM EDTA as in step 3 above.

5. Freeze samples at −80°C until analysis or proceed directly to Section 2.3.3.

2.3.3 Nonreducing SDS-PAGE immunoblotting and quantitation of crosslinking

1. Thaw frozen samples on ice if necessary.

2. Add 17.5 μL of 5 × nonreducing SDS loading buffer to each sample. Boil for exactly 3 min (see Note 7).

3. Load 15 μL of each sample onto a 10% Tris–glycine SDS-polyacrylamide gel. If reduced and nonreduced samples will be loaded on the same gel, it is best to leave an empty lane between them to avoid diffusion of DTT into nonreduced sample lanes during electrophoresis.

4. Subsequent steps of gel electrophoresis, protein electrotransfer to polyvinylidene difluoride (PVDF) membranes (Millipore Sigma), and immunodetection follow standard procedures. Perform immunoblotting against the V5 epitope on Rpn7 and against G6PD as a loading control.

5. Using image quantitation software, measure the volume of the crosslinked and uncrosslinked Rpn7 signal for each lane (see Note 8).

6. The volume of the crosslinked band divided by the sum of the crosslinked and uncrosslinked volumes, multiplied by 100, yields the percent subunit crosslinking.
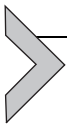
3. Assessing the impact of proteasomal peptidase inhibitor bortezomib on 26S proteasome conformational distribution

Some proteasomal peptidase inhibitors bias the conformational distribution of 26S proteasomes toward the activated states (Haselbach et al., 2017). The methodology in Section 2 can be readily modified to assess the impact of such inhibitors on the conformational distribution of the 26S proteasome. We have accomplished this as described below via pretreatment of WCE with the desired inhibitor(s) prior to crosslinking and analysis, but in principle cells could instead be treated with inhibitor prior to generation of cell extracts. By performing the crosslinking in the presence of the inhibitor and either ATP or a hydrolysis-resistant analog

such as ATPγS or AMP-PNP, inhibitor bias toward or away from the s1 conformation can be assessed. Concurrent measurement of peptidase activity inhibition in an aliquot of the treated lysates using a fluorogenic substrate such as *N*-succinyl-leu-leu-val-tyr-7-amino-4-methylcoumarin (suc-LLVY-AMC) serves to confirm the inhibitor is bound to proteasomes under the crosslinking conditions (see Note 9). We demonstrate this approach using the FDA-approved proteasome inhibitor bortezomib as an example.

3.1 Materials

- Materials described in Section 2.1
- 10 mM bortezomib (Selleckchem): dissolve in anhydrous dimethylsulfoxide (DMSO) and store in single-use aliquots at −80°C. This reagent is stable for at least 6 months
- 2.5 mM suc-LLVY-AMC (R&D Systems): dissolve in anhydrous DMSO and store in single-use aliquots at −80°C. This reagent is stable for at least a year
- Black polystyrene 384-well plates (Corning Life Sciences)

3.2 Equipment

- Equipment described in Section 2.2
- Temperature-controlled multiwell fluorescence plate reader capable of reading 384-well plates and equipped with appropriate optics for imaging AMC fluorescence (BioTek Synergy H1 or similar)

3.3 Procedure

3.3.1 Disulfide crosslinking of vehicle- or bortezomib-treated WCE

1. Overnight yeast cultures are grown as in Section 2.3.1, but are diluted into 30 mL of culture instead of 15 mL. One culture for DMSO vehicle and one for bortezomib treatment should be prepared.
2. Cell harvest is performed as in Section 2.3.1, except 20 mL of culture is harvested instead of 10 mL.
3. Spheroplasting and lysis are performed as in Section 2.3.1, except the reagent volumes listed in steps 6, 8, 9, and 10 are doubled.
4. Add 3 μL of DMSO or bortezomib (final concentration 100 μM) to 300 μL of the appropriate WCE and mix gently but thoroughly. Incubate on ice for 5 min.

5. Set ~160 μL of the treated WCE aside at 4°C for measurement of peptidase activity (Section 3.3.2).

6. Using the remaining WCE, perform crosslinking and analysis as in Sections 2.3.2 and 2.3.3.

3.3.2 Confirming proteasome inhibition via fluorogenic substrate cleavage assay

1. Transfer 50 μL of uncrosslinked, vehicle- or inhibitor-treated WCE from Section 3.3.1, step 5 to each of three wells of a 384-well black polystyrene microplate.

2. Add 1 μL of 2.5 mM suc–LLVY–AMC to each well. Mix thoroughly by pipetting up and down without introducing bubbles.

3. Measure fluorescence resulting from cleavage of suc–LLVY–AMC at excitation 360 nm, emission 460 nm at 30°C every minute for 60 min using the multiwell fluorescence plate reader.

4. Average the three readings for each sample and plot the average fluorescence intensity in arbitrary units vs time in minutes for the first 20 time points. Calculate the slope of the line to establish the peptidase rate in arbitrary fluorescence units per minute (see Note 10). Inhibition of peptidase activity by ≈90% is anticipated (some minimal fluorescence liberation by other cellular peptidases is typical).

4. Summary and conclusion

Cryo-EM has been enormously powerful in documenting the conformational states of multisubunit complexes. However, it requires access to extremely expensive equipment and the preparation of highly pure samples. Further, data processing is time- and effort-intensive, resulting in limited throughput that hinders detailed comparative mechanistic studies. The crosslinking approach described here circumvents each of these limitations and thus provides a powerful means to rapidly and efficiently compare many samples in parallel. Further, because it relies on methods and equipment that are already available in most molecular biology labs, it can be broadly implemented to study any multisubunit protein complex for which high resolution structures of multiple conformational states are known.

An additional advantage of this approach is that, due to the precise amino acid spacing necessary for disulfide bond formation (~5.9 Å between cysteine α carbons), smaller conformational changes can be measured than are possible with several other methods. For example, Förster resonance energy

transfer is widely used to measure protein conformational changes, but is restricted to movements on the order of ∼20–100 Å (Heyduk, 2002). In contrast, the Rpn6(T203C)–Rpt6(G387C) crosslinker pair described above discriminates a movement of ∼9 Å between the s1 and s2/s3-like states (Eisele et al., 2018). Theoretically, any pair of residues whose α carbons are spaced ∼5–6 Å apart in one conformation and >10–15 Å in another can constitute a reporter pair upon cysteine substitution. In practice, these distance constraints are influenced by the local flexibilities of the protein regions in which the residues are located, and this should be considered when choosing sites for cysteine substitution.

Typical results for ATP analogs (Fig. 2A) and for bortezomib treatment (Fig. 2B and C) are shown. Crosslinking efficiency of the Rpn7(D123C)–Rpt2(R407C) reporter typically ranges from <3% in the presence of high concentrations of ATPγS or AMP-PNP to approximately 30% in the presence of ATP and is highly reproducible. Incomplete crosslinking in the presence of ATP is likely due to a combination of incomplete conformational switching, imperfect alignment or spacing of cysteines for disulfide formation (see below), or spontaneous oxidation of cysteines prior to crosslinking. Generally, our efforts to further enhance the efficiency via extended crosslinking time courses or use of other oxidants have not been effective.

Although the utility of this crosslinking-based approach has been established (Eisele et al., 2018), there are two potential limitations that should be carefully considered before use. First, the assay is not time–resolved. Specifically, it reports on all proteasomes cycling through the s1 state over the course of crosslinking. Thus, fast rearrangements may be difficult to capture and quantitate accurately via this approach. For this reason, we have had the greatest success using this approach in combination with chemicals or mutations that arrest particular enzymatic activities of the proteasome, as they often trap particular conformational states or distributions.

The second consideration is that disulfide formation is dependent on precise juxtaposition of cysteine residues. Although this means that crosslinking is highly selective for a particular conformation or subunit juxtaposition, it also means that small perturbations to the positioning of an engineered cysteine-containing subunit may alter the crosslinking efficiency due to relatively small changes in the positions of the engineered cysteines. The resultant loss or gain of crosslinking could thus be misidentified as global changes to the conformational state. For this reason, we recommend using multiple pairs of engineered cysteines, ideally present in different subunits and regions of the multisubunit complex, to validate the initial results whenever possible (Eisele et al., 2018).
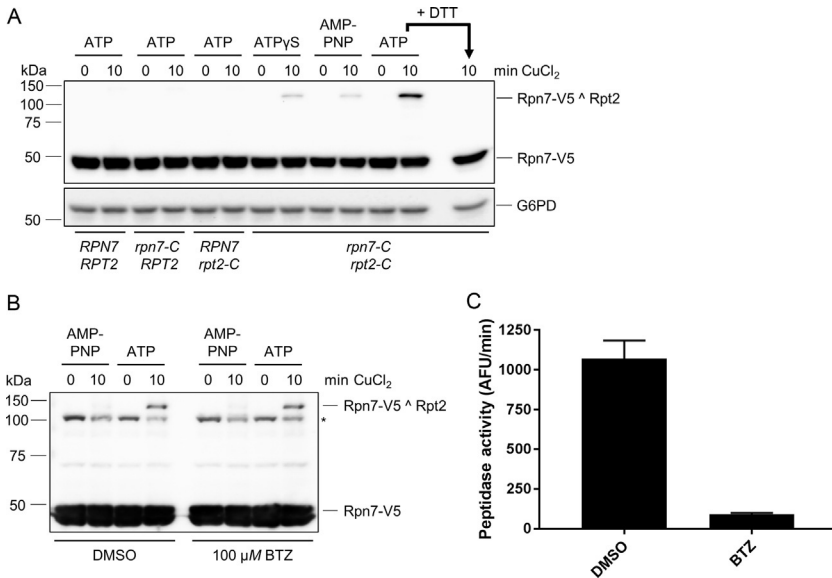
Fig. 2 (A) Conformation-dependent crosslinking of Rpn7 and Rpt2. Crosslinking requires both engineered cysteines and is regulated by nucleotide. Crosslinking was induced in the presence of 2mM of the indicated nucleotide. For the last lane, the WCE was pre-incubated with DTT to reduce disulfide crosslinks prior to loading. (B) Bortezomib (BTZ) treatment does not influence Rpn7-Rpt2 crosslinking. Extracts from DMSO- or BTZ- (100 μM) treated cells were crosslinked as in (A) in the presence of 2mM ATP or AMP-PNP as shown. *Asterisk*, nonspecific cross-reacting band occasionally seen with V5 antibody. (C) Measurement of proteasomal peptidase activity in extracts from (B). Cell extract (20 μg) from DMSO- or BTZ-treated cells was incubated with 50 μM suc-LLVY-AMC for 60 min at 30°C and fluorescence from liberated AMC was measured. The rate of fluorescence liberation is shown. *AFU*, arbitrary fluorescence units. Error bars indicate standard deviations ($N = 5$). *Panel (A) is modified from Eisele, M. R., Reed, R. G., Rudack, T., Schweitzer, A., Beck, F., Nagy, I., et al. (2018). Expanded coverage of the 26S proteasome conformational landscape reveals mechanisms of peptidase gating. Cell Reports, 24(5), 1301–1315.e5. doi:10.1016/j.celrep.2018.07.004 with permission from Elsevier.*

5. Notes

1. The cells are no longer protected by the cell wall and are now very fragile. Handle gently to prevent premature cell lysis.

2. Samples should be kept on ice at all times from this step forward to limit proteolysis and spontaneous oxidation of cysteines.

3. To ensure reproducible crosslinking efficiency both between samples and from experiment to experiment, we routinely dilute our extracts to 4 mg/mL prior to crosslinking.

4. Although we prefer CuCl$_2$ as the mild oxidant to induce disulfide formation, many other commercially available oxidants can be used. Examples include tetrathionate and aqueous iodine, both of which have been used successfully to induce disulfide crosslinks in proteasome complexes (Snoberger, Brettrager, & Smith, 2018; Velichutina et al., 2004).

5. Some engineered cysteines are prone to spontaneous disulfide formation even in the absence of exogenous oxidant, which can confound interpretation of crosslinking results. This spontaneous oxidation can be minimized by incubating the samples on ice instead of 25°C during crosslinking. We have generally found that there is no need to extend the crosslinking time to accommodate for the decrease in temperature.

6. Typically, maximal crosslinking occurs in less than 5 min, and that nonspecific crosslinking increases over time. For this particular crosslink pair, 10 min consistently provides near-maximal site-specific crosslinking efficiency with minimal nonspecific crosslinking. If desired, a crosslinking time course can be used to optimize the results for this and other cysteine pairs.

7. Despite the presence of NEM and EDTA that should prevent further oxidation of free protein thiols, we have found that extensive boiling, as well as repeated boiling, of nonreducing SDS-PAGE samples leads to additional nonspecific disulfide formation over time, possibly due to incomplete reaction of NEM with free thiols. For this reason, we carefully control the boiling time and make aliquots of crosslinked samples prior to freezing if multiple analyses are planned.

8. It is critical to use images in which the signals for both the uncrosslinked and crosslinked subunits are unsaturated to ensure accurate calculation of crosslinking efficiency. Most modern biomedical imaging systems have very large dynamic ranges and automatically detect and alert the user to signal saturation. For this reason, such imagers are preferred over autoradiography film.

9. Bortezomib preferentially inhibits the chymotryptic-like activity of the proteasome. The fluorogenic substrate suc-LLVY-AMC reports on this chymotryptic-like activity. If inhibitors of the trypsin-like or caspase-like activities of the proteasome will be assayed instead, fluorogenic substrates suitable for those activities should be substituted for suc-LLVY-AMC.

10. It is important that peptidase assays are performed under conditions where substrate is in great molar excess of proteasomes to ensure a linear relationship between fluorescence liberation and time. If substantial deviation from linearity is observed over the first 20 min of the assay, then the concentration of the extracts used in the assay should be reduced.

Acknowledgments

References

Asano, S., Fukuda, Y., Beck, F., Aufderheide, A., Forster, F., Danev, R., et al. (2015). Proteasomes. A molecular census of 26S proteasomes in intact neurons. *Science*, *347*(6220), 439–442. https://doi.org/10.1126/science.1261197.

Aufderheide, A., Beck, F., Stengel, F., Hartwig, M., Schweitzer, A., Pfeifer, G., et al. (2015). Structural characterization of the interaction of Ubp6 with the 26S proteasome. *Proceedings of the National Academy of Sciences of the United States of America*, *112*(28), 8626–8631. https://doi.org/10.1073/pnas.1510449112.

Bard, J. A. M., Bashore, C., Dong, K. C., & Martin, A. (2018). Deconvolution of substrate processing by the 26S proteasome reveals a selective kinetic gateway to degradation. *bioRxiv*. https://doi.org/10.1101/359695.

Bard, J. A. M., Goodall, E. A., Greene, E. R., Jonsson, E., Dong, K. C., & Martin, A. (2018). Structure and function of the 26S proteasome. *Annual Review of Biochemistry*, *87*, 697–724. https://doi.org/10.1146/annurev-biochem-062917-011931.

Bashore, C., Dambacher, C. M., Goodall, E. A., Matyskiela, M. E., Lander, G. C., & Martin, A. (2015). Ubp6 deubiquitinase controls conformational dynamics and substrate degradation of the 26S proteasome. *Nature Structural & Molecular Biology*, *22*(9), 712–719. https://doi.org/10.1038/nsmb.3075.

Chen, S., Wu, J., Lu, Y., Ma, Y. B., Lee, B. H., Yu, Z., et al. (2016). Structural basis for dynamic regulation of the human 26S proteasome. *Proceedings of the National Academy of Sciences of the United States of America*, *113*(46), 12991–12996. https://doi.org/10.1073/pnas.1614614113.

de la Pena, A. H., Goodall, E. A., Gates, S. N., Lander, G. C., & Martin, A. (2018). Substrate-engaged 26S proteasome structures reveal mechanisms for ATP-hydrolysis-driven translocation. *Science*. https://doi.org/10.1126/science.aav0725. [Epub ahead of print].

Dong, Y., Zhang, S., Wu, Z., Li, X., Wang, W. L., Zhu, Y., et al. (2018). Visualizing ATP-dependent substrate-processing dynamics of the human 26S proteasome at near-atomic resolution. *bioRxiv*. https://doi.org/10.1101/419051.

Eisele, M. R., Reed, R. G., Rudack, T., Schweitzer, A., Beck, F., Nagy, I., et al. (2018). Expanded coverage of the 26S proteasome conformational landscape reveals mechanisms of peptidase gating. *Cell Reports*, *24*(5), 1301–1315.e5. https://doi.org/10.1016/j.celrep.2018.07.004.

Finley, D., Chen, X., & Walters, K. J. (2016). Gates, channels, and switches: Elements of the proteasome machine. *Trends in Biochemical Sciences*, *41*(1), 77–93. https://doi.org/10.1016/j.tibs.2015.10.009.

Guo, Q., Lehmer, C., Martinez-Sanchez, A., Rudack, T., Beck, F., Hartmann, H., et al. (2018). In situ structure of neuronal C9orf72 poly-GA aggregates reveals proteasome recruitment. *Cell*, *172*(4), 696–705.e12. https://doi.org/10.1016/j.cell.2017.12.030.

Haselbach, D., Schrader, J., Lambrecht, F., Henneberg, F., Chari, A., & Stark, H. (2017). Long-range allosteric regulation of the human 26S proteasome by 20S proteasome-targeting cancer drugs. *Nature Communications*, *8*, 15578. https://doi.org/10.1038/ncomms15578.

Heyduk, T. (2002). Measuring protein conformational changes by FRET/LRET. *Current Opinion in Biotechnology*, *13*(4), 292–296. https://doi.org/10.1016/S0958-1669(02)00332-4.

Huang, X., Luan, B., Wu, J., & Shi, Y. (2016). An atomic structure of the human 26S proteasome. *Nature Structural & Molecular Biology*, *23*(9), 778–785. https://doi.org/10.1038/nsmb.3273.

Luan, B., Huang, X., Wu, J., Mei, Z., Wang, Y., Xue, X., et al. (2016). Structure of an endogenous yeast 26S proteasome reveals two major conformational states. *Proceedings of the National Academy of Sciences of the United States of America*, *113*(10), 2642–2647. https://doi.org/10.1073/pnas.1601561113.

Matyskiela, M. E., Lander, G. C., & Martin, A. (2013). Conformational switching of the 26S proteasome enables substrate degradation. *Nature Structural & Molecular Biology*, *20*(7), 781–788. https://doi.org/10.1038/nsmb.2616.

Schweitzer, A., Aufderheide, A., Rudack, T., Beck, F., Pfeifer, G., Plitzko, J. M., et al. (2016). Structure of the human 26S proteasome at a resolution of 3.9 A. *Proceedings of the National Academy of Sciences of the United States of America*, *113*(28), 7816–7821. https://doi.org/10.1073/pnas.1608050113.

Sledz, P., Unverdorben, P., Beck, F., Pfeifer, G., Schweitzer, A., Forster, F., et al. (2013). Structure of the 26S proteasome with ATP-gammaS bound provides insights into the mechanism of nucleotide-dependent substrate translocation. *Proceedings of the National Academy of Sciences of the United States of America*, *110*(18), 7264–7269. https://doi.org/10.1073/pnas.1305782110.

Snoberger, A., Brettrager, E. J., & Smith, D. M. (2018). Conformational switching in the coiled-coil domains of a proteasomal ATPase regulates substrate processing. *Nature Communications*, *9*(1), 2374. https://doi.org/10.1038/s41467-018-04731-6.

Tomko, R. J., Jr., Funakoshi, M., Schneider, K., Wang, J., & Hochstrasser, M. (2010). Heterohexameric ring arrangement of the eukaryotic proteasomal ATPases: Implications for proteasome structure and assembly. *Molecular Cell*, *38*(3), 393–403. https://doi.org/10.1016/j.molcel.2010.02.035.

Tomko, R. J., Jr., & Hochstrasser, M. (2013). Molecular architecture and assembly of the eukaryotic proteasome. *Annual Review of Biochemistry*, *82*, 415–445. https://doi.org/10.1146/annurev-biochem-060410-150257.

Unverdorben, P., Beck, F., Sledz, P., Schweitzer, A., Pfeifer, G., Plitzko, J. M., et al. (2014). Deep classification of a large cryo-EM dataset defines the conformational landscape of the 26S proteasome. *Proceedings of the National Academy of Sciences of the United States of America*, *111*(15), 5544–5549. https://doi.org/10.1073/pnas.1403409111.

Velichutina, I., Connerly, P. L., Arendt, C. S., Li, X., & Hochstrasser, M. (2004). Plasticity in eucaryotic 20S proteasome ring assembly revealed by a subunit deletion in yeast. *The EMBO Journal*, *23*(3), 500–510. https://doi.org/10.1038/sj.emboj.7600059.

Verma, R., Aravind, L., Oania, R., McDonald, W. H., Yates, J. R., 3rd, Koonin, E. V., et al. (2002). Role of Rpn11 metalloprotease in deubiquitination and degradation by the 26S proteasome. *Science*, *298*(5593), 611–615. https://doi.org/10.1126/science.1075898.

Wehmer, M., Rudack, T., Beck, F., Aufderheide, A., Pfeifer, G., Plitzko, J. M., et al. (2017). Structural insights into the functional cycle of the ATPase module of the 26S proteasome. *Proceedings of the National Academy of Sciences of the United States of America*, *114*(6), 1305–1310. https://doi.org/10.1073/pnas.1621129114.

Worden, E. J., Dong, K. C., & Martin, A. (2017). An AAA motor-driven mechanical switch in Rpn11 controls deubiquitination at the 26S proteasome. *Molecular Cell*, *67*(5), 799–811.e8. https://doi.org/10.1016/j.molcel.2017.07.023.

Yao, T., & Cohen, R. E. (2002). A cryptic protease couples deubiquitination and degradation by the proteasome. *Nature*, *419*(6905), 403–407. https://doi.org/10.1038/nature01071.

Zhu, Y., Wang, W. L., Yu, D., Ouyang, Q., Lu, Y., & Mao, Y. (2018). Structural mechanism for nucleotide-driven remodeling of the AAA-ATPase unfoldase in the activated human 26S proteasome. *Nature Communications*, *9*(1), 1360. https://doi.org/10.1038/s41467-018-03785-w.